

Graph-Based Joint Dequantization and Contrast Enhancement of Poorly Lit JPEG Images

Xianming Liu^{ID}, Member, IEEE, Gene Cheung^{ID}, Senior Member, IEEE, Xiangyang Ji^{ID}, Member, IEEE,
Debin Zhao^{ID}, Member, IEEE, and Wen Gao, Fellow, IEEE

Abstract—JPEG images captured in poor lighting conditions suffer from both low luminance contrast and coarse quantization artifacts due to lossy compression. Performing dequantization and contrast enhancement in separate back-to-back steps would amplify the residual compression artifacts, resulting in low visual quality. Leveraging on recent development in graph signal processing (GSP), we propose to jointly dequantize and contrast-enhance such images in a single graph-signal restoration framework. Specifically, we separate each observed pixel patch into illumination and reflectance via Retinex theory, where we define generalized smoothness prior and signed graph smoothness prior according to their respective unique signal characteristics. Given only a transform-coded image patch, we compute robust edge weights for each graph via low-pass filtering in the dual graph domain. We compute the illumination and reflectance components for each patch alternately, adopting accelerated proximal gradient (APG) algorithms in the transform domain, with backtracking line search for further speedup. Experimental results show that our generated images outperform the state-of-the-art schemes noticeably in the subjective quality evaluation.

Index Terms—Contrast enhancement, de-quantization, image decomposition, graph signal restoration.

I. INTRODUCTION

THOUGH small cameras on mobile devices like phones and tablets are now ubiquitous, in practice photos are often taken haphazardly in non-ideal conditions, e.g., poorly lit dark rooms. Given a captured image with low lighting contrast,

Manuscript received May 19, 2018; revised September 19, 2018; accepted September 23, 2018. Date of publication September 28, 2018; date of current version November 2, 2018. This work was supported in part by the Major State Basic Research Development Program of China under Grant 973 Program 2015CB351804, in part by the National Science Foundation of China under Grant 61672193, Grant 61502122, and Grant 61620106005, in part by the Fundamental Research Funds for the Central Universities under Grant HIT.NSRIF.2015067, and in part by the Tsinghua University Initiative Scientific Research Program. The associate editor coordinating the review of this manuscript and approving it for publication was Prof. Xiaochun Cao. (*Corresponding author: Xianming Liu*)

X. Liu and D. Zhao are with the School of Computer Science and Technology, Harbin Institute of Technology, Harbin 150001, China, and also with the Peng Cheng Laboratory, Shenzhen 518052, China (e-mail: csxm@hit.edu.cn; dbzhao@hit.edu.cn).

G. Cheung is with the Department of Electrical Engineering & Computer Science, York University, Toronto, ON M3J 1P3, Canada (e-mail: genec@yorku.ca).

X. Ji is with the Department of Automation, Tsinghua University, Beijing 100084, China (e-mail: xyji@tsinghua.edu.cn).

W. Gao is with the School of Electrical Engineering and Computer Science, Peking University, Beijing 100871, China, and also with the Peng Cheng Laboratory, Shenzhen 518052, China (e-mail: wgao@pku.edu.cn).

Color versions of one or more of the figures in this paper are available online at <http://ieeexplore.ieee.org>.

Digital Object Identifier 10.1109/TIP.2018.2872871

typically contrast enhancement techniques are applied, most of which assume that the input image is noiseless [1]–[5]. However, the majority of the images captured by consumer-level mobile devices are compressed by JPEG [6], the most prevalent image coding standard, to reduce storage / Internet bandwidth cost. Compression artifacts, such as blocking and ringing, are induced due to coarse quantization of discrete cosine transform (DCT) coefficients. Thus the noiseless assumption is typically not true in practice.

To handle both low light contrast and quantization effects, one naive approach is to first perform state-of-the-art dequantization (also known as *soft decoding*) on the JPEG image [7], [8], then perform contrast enhancement. However, residual compression artifacts in dark regions would be amplified during enhancement, resulting in poor visual quality. On the other hand, if one performs contrast enhancement on a decoded JPEG image then employs a deblocking procedure in the pixel domain like [9], then the deblocking procedure may destroy image details along block boundaries.

Leveraging on recent progress on *graph signal processing* (GSP) [10], [11], in this paper we propose a unified graph-based Retinex optimization framework that mitigates quantization noise and boosts lighting contrast at the same time. Specifically, we decompose an observed image patch into a pixel-by-pixel product of two components, *illumination* and *reflectance*, each of which has unique characteristics (spatially smooth and piecewise smooth respectively) that can be elegantly described as novel smoothness priors for signals on graphs. In particular, for illumination we define a *generalized graph smoothness prior* that is a generalization of *total generalized variation* (TGV) [12] that considers higher-order smoothness to the graph-signal domain.

For reflectance we construct *signed graphs* [13] with both positive edges (to average out quantization noise among different pixels) and negative edges (to accentuate the difference between connected pixel pairs) to describe the desired patch structure, so that the dequantized and contrast-enhanced patch can be computed in a unified optimization formulation. Edge weights are estimated efficiently and robustly via low-pass filtering in the dual graph domain [14]. Unlike commonly used total variation (TV) and variants [5], [15] that are convex but non-differentiable l_1 norms, our proposed graph smoothness priors for illumination and reflectance can be computed as convex and differentiable weighted l_2 norms in each iteration, leading to intuitive and simple optimization.

Given quantization bin constraints, we compute illumination and reflectance components for each patch alternately using our designed *accelerated proximal gradient* (APG) algorithms [16] in the DCT transform domain, with backtracking line search for further speedup. We derive a contrast boost factor per patch via global contrast-tone mapping [3]. Experimental results show that our proposed algorithm outperforms competing schemes noticeably in subjective quality evaluation. Our technical contributions can be summarized as follow:

- 1) We define graph-signal smoothness priors that simply and accurately modeled the unique characteristics of illumination and reflectance components of pixel patches in a natural image;
- 2) We compute edge weights for the illumination and reflectance components robustly via a simple optimization in the dual-graph domain;
- 3) We design fast APG algorithms in the transform domain to optimize the illumination and reflectance components alternately; and
- 4) We demonstrate through extensive subjective experiments that our dequantized and contrast-enhanced images are visually more pleasing than competing schemes.

The outline of the paper is as follows. We overview relate work in Section II, then introduce the related preliminaries in Section III, including image formation model, quantization bin constraint and background for GSP. In Section IV, we define signal priors for illumination and reflectance, and formulate our optimization objective. We describe our optimization algorithm in Section V. Finally, experimental results and conclusions are presented in Section VI and VII, respectively.

II. RELATED WORK

We briefly overview related works to our proposed method on three main aspects: 1) Retinex model based contrast enhancement; 2) JPEG-compressed image dequantization; and 3) graph-based image restoration.

A. Retinex Model Based Contrast Enhancement

The goal of contrast enhancement is to adjust the illumination distribution of an image to make more image details visible. In image decomposition based contrast enhancement, the Retinex model is the most popular underlying model, which assumes that an image is a product of the illumination intensity and the underlying reflectance of the object. Retinex model based decomposition is to separate illumination from reflectance, which enables the reprojection of alternative lighting, and thus has been widely adopted for image contrast enhancement [1], [2], [5], [15], [17].

Estimating illumination and reflectance components from a single image is an ill-posed problem. To make the problem trackable, some methods casted the illumination / reflectance decomposition as a statistical inference problem by posing different priors on illumination and reflectance, and defined a variational optimization to search for the most likely

solutions. For instance, Ng and Wang [2] assumed that the reflectance is *piecewise constant* (PWC), and employed *total-variation* (TV) to regularize reflectance. However, this assumption of reflectance is too stringent, resulting in over-smoothed images. Fu *et al.* [4] showed that the linear domain model can better represent the prior information of [2] than the logarithmic domain to achieve better estimation of reflectance and illumination. Recently, in [15], to better separate illumination and reflectance, Yue *et al.* introduced a weighted ℓ_1 -norm on neighboring pixels according to the color similarity for computing the reflectance layer. Guo *et al.* [5] proposed a weighted TV model to promote structure-aware smoothing for computing illumination.

After illumination / reflectance decomposition, traditional Retinex-based methods directly utilize the decomposed reflectance layer as the enhanced result [18], [19]. However, these approaches often result in unnatural enhanced images. Many algorithms compensate illumination by gamma correction to enhance the contrast [4], [5], [15]. However, These methods all assume that the input image is uncompressed and noiseless. In practice, almost all images obtained from the Internet or consumer imaging devices are compressed to reduce storage cost. Subsequent gamma correction thus amplifies compression artifacts hidden in dark regions, damaging the resulting image reconstruction quality. Li *et al.* [20] decomposed an image into structure (*i.e.*, the main objects) and texture (*i.e.*, the fine details) and processed them separately. However, [20] failed to boost the contrast of images well due to the limitation of the adopted tone-curve function. Instead, we propose a unified optimization, which suppresses compression artifacts in the illumination / reflectance components and boosts contrast simultaneously.

It should be noted that, for decomposition based image enhancement, often physically accurate estimates are not necessary; a physically plausible estimate that satisfies the prior assumptions leading to good visual quality is already sufficient.

B. Restoration of JPEG-Compressed Images

There are two general approaches to restore a compressed JPEG image in the literature: deblocking [9] and soft decoding [7], [8], [21], [22].

Since JPEG compresses each non-overlapping block independently, the most noticeable compression artifact is blocking artifact. Deblocking attempts to remove compression noise along block boundaries. A straightforward idea is to perform low-pass filtering to suppress structured discontinuities induced by code blocks. For instance, Zhai *et al.* [23] employed post-filtering in shifted overlapped windows and fused the filtering results to better suppress blocking artifacts. This approach only exploits the correlations among inter-blocks, and thus has limited restoration performance. There are also deblocking methods work on decoded JPEG image directly, and recovers it in a similar way as denoising via pre-defined prior models, by regarding compression noise as additive white Gaussian noise. For example, Foi *et al.* [9] designed powerful image filtering algorithms based on shape-adaptive

DCT (SA-DCT). By using arbitrarily-shaped supports which are adaptive with respect to the image, the reconstructed edges are clean, and no unpleasant ringing artifacts are introduced by the fitted transform.

Soft decoding, also called dequantization, is a more powerful strategy to combat quantization noise. In contrast to hard decoding, soft decoding only constrains each DCT coefficient to be within the indexed quantization bin, but choose the most probable one with the help of natural image statistics. It utilizes all available information such as quantization bin constraint and natural image priors for optimization, and hence has potential to achieve better restoration performance. The challenge of soft decoding thus lies in identifying appropriate signal priors and incorporating them into an effective restoration algorithm. For instance, to reduce blocking artifacts and Gibbs phenomenon while preserving sharp edges, Alter *et al.* proposed to combine the classical total variation (TV) prior with the quantization constraint [24], by assuming that natural images are approximately piecewise constant. Zhang *et al.* [7] exploited the non-local self-similarity characteristic in DCT domain constrained by the intervals of unquantized DCT coefficients. This scheme achieves state-of-the-art soft decoding performance. Liu *et al.* [25] proposed to exploit residual redundancies of JPEG code streams and sparsity properties of latent images. The restoration is a sparse coding process carried out jointly in the DCT and pixel domains.

C. Graph-Based Image Restoration

Recent interest in *graph signal processing* (GSP) [10] has led to spectral analysis tools like transforms [26], [27] and wavelets to process signals living on irregular data kernels described by graphs. Though pixels in an image are regular samples on a 2D grid, one can nonetheless interpret an image (patch) as a sparsely connected graph and leverage GSP tools for signal analysis and restoration, as done in [8], [14], and [28] for image denoising and dequantization of JPEG images. Extending these works, in the paper we construct an appropriate *signed graph* [13] for joint image denoising and contrast enhancement, where positive edges connect pixels for averaging, and negative edges connect pixels to accentuate their inter-pixel differences. *To the best of our knowledge, we are the first in the GSP literature to use signed graphs for image restoration problems.*

III. PRELIMINARIES

A. Image Formation Model

Following the seminal work on Retinex theory [1], we assume that an ideal image is an element-by-element multiplication of illumination and reflectance images. We thus employ the following image formation model, previously proposed in Retinex-based image decomposition literature [1], [2], [5], [15], [17], for an N -pixel patch $\mathbf{y} \in \mathbb{R}^N$ in a dark captured image:

$$\mathbf{y} = \tau \mathbf{l} \odot \mathbf{r} + \mathbf{z} \quad (1)$$

where operator \odot denotes element-by-element multiplication, and \mathbf{r} , \mathbf{l} and \mathbf{z} , all in \mathbb{R}^N , are the reflectance, illumination

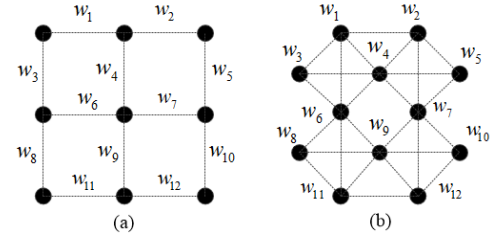


Fig. 1. Examples of original pixel graph \mathcal{G} and dual edge weight graph \mathcal{G}^d : (a) 9-node original graph, (b) 12-node dual graph.

and additive noise, respectively. $0 < \tau \leq 1$ is a *contrast reduction factor* modeling the dark image capture environment and varies patch-by-patch. While \mathbf{r} and \mathbf{l} are computed *locally* for every patch, τ is pre-selected per-patch *globally* based on statistics of the entire image via contrast-tone mapping [3].

B. Quantization Bin Constraint

A captured image is usually compressed to reduce storage cost. JPEG is still currently the most prevalent compression format for images. In JPEG standard, each non-overlapping 8×8 pixel block—called a *code block*—in an image is compressed independently via transform coding. Specifically, each code block in vector form $\mathbf{y} \in \mathbb{R}^{64}$ is transformed via DCT to 64 coefficients $\mathbf{Y} = \mathbf{T}\mathbf{y}$, where \mathbf{T} is the transform matrix. The i -th coefficient Y_i is quantized using *quantization parameter* (QP) Q_i —assigned a quantization bin (*q-bin*) index $q_i \in \mathbb{Z}$ (*q-index*) as: $q_i = \text{round}(Y_i/Q_i)$. At the decoder, having received only q-index q_i there exists an uncertainty when recovering Y_i :

$$\left(q_i - \frac{1}{2}\right) Q_i \leq Y_i < \left(q_i + \frac{1}{2}\right) Q_i. \quad (2)$$

This quantization constraint defines the search space for Y_i during restoration of the code block.

C. Graph-Based Image Priors

In the Retinex literature [1], [2], illumination is assumed to vary slowly across spatial dimensions, while a reflectance image is known to be *piecewise smooth* (PWS) with occasional sharp discontinuities. We express both notions mathematically from a graph spectral perspective. Before we describe our proposed smoothness priors for the two components, we first overview some fundamental concepts in GSP.

1) *Spectral Decomposition of Graph-Signals*: We interpret a size- N pixel patch $\mathbf{x} \in \mathbb{R}^N$ as a signal on top of a graph $\mathcal{G}(\mathcal{N}, \mathcal{E})$ with N nodes \mathcal{N} and edges \mathcal{E} , where each pixel in \mathbf{x} is represented by a node in \mathcal{N} and is connected to its four nearest pixels with edges (horizontal and vertical neighbors), as illustrated in Fig. 1-(a). \mathcal{G} is called a *four-connected graph*. Each edge connecting pixel (node) pair i and j has weight $w_{i,j}$ that reflects the (dis)similarity or (anti-)correlation between the pair's pixel values, x_i and x_j . Conventionally, edge weight $w_{i,j}$ for pixel pair (i, j) is computed using *features* of the

two pixels and a Gaussian kernel, for example:

$$w_{i,j} = \exp \left\{ -\frac{\|\mathbf{c}_i - \mathbf{c}_j\|_2^2}{\sigma_l^2} \right\} \exp \left\{ -\frac{(x_i - x_j)^2}{\sigma_s^2} \right\} \quad (3)$$

where \mathbf{c}_i and x_i are the respective location and sample value of pixel i , and σ_l and σ_s are parameters. In words, (3) states that edge weight $w_{i,j}$ is large (close to 1) if the features of the pixel pair are similar, and small (close to 0) otherwise. It is akin to bilateral filter weight computation with domain and range filters [29].

Given $w_{i,j}$, the *adjacency matrix* \mathbf{W} , where $W_{i,j} = w_{i,j}$, and the diagonal *degree matrix* \mathbf{D} , where $D_{i,i} = \sum_j W_{i,j}$, can be defined. Finally, the combinatorial *graph Laplacian matrix* is defined as $\mathbf{L} = \mathbf{D} - \mathbf{W}$ [30]–[33]. Because \mathbf{L} is symmetric and real, it can be eigen-decomposed into orthogonal vectors with real eigenvalues, *i.e.*, $\mathbf{V}\Lambda\mathbf{V}^\top = \mathbf{L}$ where Λ is a diagonal matrix with eigenvalues λ_k on the diagonal. We interpret eigenvalues λ_k and eigenvectors \mathbf{v}_k as *graph frequencies* and *graph frequency components* respectively that define the spectrum for graph \mathcal{G} . Any graph-signal \mathbf{x} on \mathcal{G} can thus be decomposed into its graph frequency components as: $\mathbf{V}^\top \mathbf{x} = \mathbf{a}$, and $\mathbf{x} = \sum_k a_k \mathbf{v}_k$, where a_k is the coefficient of graph frequency k for \mathbf{x} . \mathbf{V}^\top is commonly called the *Graph Fourier Transform* (GFT) [10], a generalization of known transforms like discrete Fourier transform (DFT) to the graph domain.

2) *Graph-Signal Smoothness Prior*: A signal \mathbf{x} is *smooth* with respect to the underlying graph \mathcal{G} if connected pairs (i, j) in \mathcal{G} with large edge weights $w_{i,j}$ have similar sample values. In the graph frequency domain, \mathbf{x} is smooth if its signal energy is concentrated mostly in the low frequencies. We can express this graph-signal smoothness notion using the *graph Laplacian regularizer* (GLR) [28]:

$$\mathbf{x}^\top \mathbf{L} \mathbf{x} = \sum_{i,j} w_{i,j} (x_i - x_j)^2 = \sum_k \lambda_k a_k^2 \quad (4)$$

We see that (4) is small if connected samples (x_i, x_j) are similar for large $w_{i,j} > 0$, or if squares of GFT coefficients a_k^2 are small for large graph frequencies λ_k .

If edge weights $w_{i,j}$ are not fixed but are functions of the sought-after signal \mathbf{x} as expressed in (3), then matrix $\mathbf{L}(\mathbf{x})$ is also a function of \mathbf{x} , and GLR can be more suggestively expressed as $\mathbf{x}^\top \mathbf{L}(\mathbf{x}) \mathbf{x}$ —we call the resulting prior *reweighted graph Laplacian prior* (RGLR). RGLR has been used for image denoising [28] and soft decoding of JPEG images [8], [14]. In particular, [28] showed that RGLR promotes PWS signal behavior similar to the TV prior via a continuous domain analysis. This explains the good performance of using RGLR in previous graph-based image restoration works [8], [14], [28], as natural images tend to be PWS.

Leveraging on these previous works [8], [14], [28], in our work we propose new variants of RGLR that capture the unique characteristics of illumination and reflectance pixel patches in the Retinex model.

IV. PRIOR DEFINITION AND PROBLEM FORMULATION

We first describe the design of graph-based signal priors for illumination and reflectance pixel patches, and then describe

the formulation of our optimization objective function based on these two priors. We also discuss how to compute edge weights robustly for the graph given only noisy image data.

A. Illumination Image Prior

It is commonly assumed that the illumination image \mathbf{I} varies slowly across the spatial dimensions. To express this mathematically, [2], [4] assumed that the gradient of \mathbf{I} , $\nabla \mathbf{I}$, has a small ℓ_2 -norm. Recently, [34] argued that minimizing $\|\nabla \mathbf{I}\|_2$ leads to undesirable halo artifacts, and proposed instead to minimize ℓ_1 -norm $\|\nabla \mathbf{I}\|_1$. However, minimizing only $\|\nabla \mathbf{I}\|_1$ leads to PWS behavior, which is the same characteristic as the reflectance image, making it difficult to differentiate between the two.

In this paper, combining the merits of previous schemes, we argue that illumination should be spatially smooth in general but contains a few sharp discontinuities at the foreground / background boundaries. Denote by \mathbf{W}_l and \mathbf{D}_l the adjacency and degree matrices for a 4-connected graph \mathcal{G}_l modeling an illumination pixel patch \mathbf{I} , and by $\mathbf{L}_l = \mathbf{D}_l - \mathbf{W}_l$ the corresponding graph Laplacian matrix. (The edge weights used to define \mathbf{W}_l will be discussed shortly.) We now express the *generalized smoothness prior* of an illumination pixel patch mathematically as follow:

$$Pr_l(\mathbf{I}) = \mathbf{I}^\top (\mathbf{L}_l + \alpha \mathbf{L}_l^2) \mathbf{I} \quad (5)$$

where α is a parameter to trade off the importance of the first and second order smoothness (which is fixed as 0.1 in our method). RGLR $\mathbf{I}^\top \mathbf{L}_l \mathbf{I}$ —when graph Laplacian \mathbf{L}_l is a function of the illumination patch \mathbf{I} —promotes PWS behavior like a TV-norm as discussed earlier. In contrast, $\mathbf{I}^\top \mathbf{L}_l^2 \mathbf{I}$ promotes small changes in gradients, *i.e.*, spatially smooth behavior in \mathbf{I} , since $\mathbf{I}^\top \mathbf{L}_l^2 \mathbf{I} = \|\mathbf{L}_l \mathbf{I}\|_2^2$, the squared sum of changes in gradient of signal \mathbf{I} with respect to graph \mathcal{G}_l .

Our graph smoothness notion (5) is related to *total generalized variation* (TGV) [12] that generalizes TV to higher-order smoothness to eliminate the known undesirable staircase effect in TV when reconstructing a linear slope in an image. The difference is that we define our generalized smoothness notion (5) in the graph domain, which leads to fast computation as discussed in Section V.

B. Reflectance Image Prior

Unlike illumination, reflectance \mathbf{r} is usually considered to be PWC [2]. Different from these works, we characterize the nature of the reflectance pixel patch as PWS, which is more general than PWC.¹ Denote by \mathbf{W}_r and \mathbf{D}_r the adjacency and degree matrices for a 4-connected graph \mathcal{G}_r modeling a reflectance pixel patch \mathbf{r} , and by $\mathbf{L}_r = \mathbf{D}_r - \mathbf{W}_r$ the corresponding graph Laplacian matrix. One approach to promote PWS mathematically, as previously done in [8], [14], and [28], is to simply use the RGLR $\mathbf{r}^\top \mathbf{L}_r \mathbf{r}$ where \mathbf{L}_r is a

¹A signal that is PWC is also PWS, but a signal that is PWS is not necessarily PWC. Expressed mathematically from a GSP perspective, a signal for a graph with a negative edge connecting two positively connected subgraphs is PWC if it is *strictly* bandlimited (with energies only in the first two frequencies), and is PWS if it has energies *mostly* in the low frequencies.

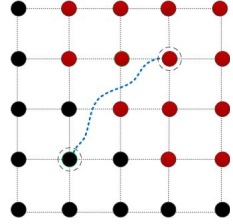


Fig. 2. Construction of centroid-connected negative graph. Pixels in a patch are firstly classified into two clusters, which are colored by black and red respectively. Then an additional negative edge (the blue dotted line) is built between two centroid nodes which are remarked by dotted circles. Nodes in each cluster are connected to their neighbors in the same cluster with positive edges.

function of the reflectance patch \mathbf{r} . To proactively sharpen contours in \mathbf{r} for contrast enhancement, we instead design \mathcal{G}_r with additional *negative edges*, *i.e.* $\exists w_{i,j} < 0$, explicitly specifying pixel pair (i, j) that are *dissimilar* and should take on very different sample values. Negative edges are used recently in data mining [13], control [35], [36] and social network analysis [37], showing that expressing dissimilarity as edges in a graphical model can improve performance in different problem domains.

In our method, a centroid-connected negative graph is constructed, as illustrated in Fig. 2. Specifically, we partition pixels in a patch into two disconnected clusters, then build an additional edge between two respective centroid nodes with a negative edge weight. Nodes in each cluster are respectively connected to their neighbors in the same cluster with positive edges. However, Laplacian \mathbf{L}_r with the additional negative edge may result in an *indefinite* matrix (*i.e.* a matrix with negative eigenvalues), and minimizing $\mathbf{r}^\top \mathbf{L}_r \mathbf{r}$ would lead to numerically unstable solutions.

To alleviate this problem, we derive a perturbation matrix $\Delta = |\lambda_{\min}^{\#}| \mathbf{I}$, where $\lambda_{\min}^{\#}$ is a lower bound for \mathbf{L}_r 's smallest negative eigenvalue λ_{\min} , *i.e.* $\lambda_{\min}^{\#} \leq \lambda_{\min} < 0$, and \mathbf{I} is an identity matrix. The perturbed matrix called the *generalized graph Laplacian* $\mathcal{L}_r = \mathbf{L}_r + \Delta$ [38] is then PSD, and GLR $\mathbf{r}^\top \mathcal{L}_r \mathbf{r}$ is lower-bounded by 0. We stress that \mathcal{L}_r preserves \mathbf{L}_r 's eigen-structure, *i.e.* eigenvectors and spacings between neighboring eigenvalues of the original \mathbf{L}_r . For a sparse symmetric matrix \mathbf{L}_r , lower bound $\lambda_{\min}^{\#}$ can be computed efficiently using a recursive algorithm [39] based on the Haynsworth inertia additivity formula [40] without full eigen-decomposition. See [39] for details.

We observe that when the negative edge weight connecting the two sub-graphs is set sufficiently small, the first eigenvector \mathbf{v}_1 of \mathcal{L}_r —corresponding to eigenvalue 0—is PWS, and the second eigenvector \mathbf{v}_2 of \mathcal{L}_r is a constant vector, as shown in Fig. 3. Given that reflectance \mathbf{r} is assumed to be PWS, a linear combination of \mathbf{v}_1 and \mathbf{v}_2 alone can well approximate the target signal \mathbf{r} , and a RGLR $\mathbf{r}^\top \mathcal{L}_r \mathbf{r}$ would promote PWS behavior while sharpening the sub-graph boundary.

To intuitively illustrate the difference between positive-only and *signed* graphs (with both positive and negative edges), we plot the first two eigenvectors \mathbf{v}_1 and \mathbf{v}_2 of the graph Laplacian for two 1D 10-node graphs respectively in Fig. 3. In these ten nodes, nodes 1 through 6 share the same sample value, while nodes 7 through 10 share another value. In other

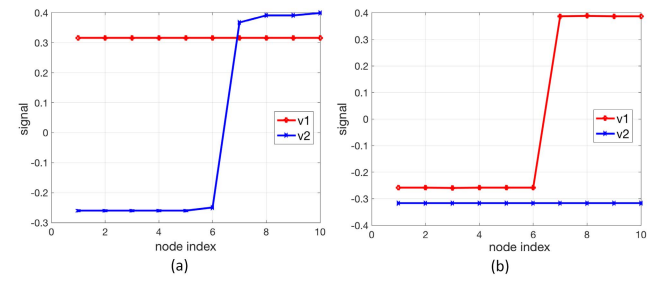


Fig. 3. The first and second eigenvectors of two 10-node 1D graphs. (a) small edge weight connecting nodes 6 and 7; (b) negative edge weight connecting nodes 3 and 8.

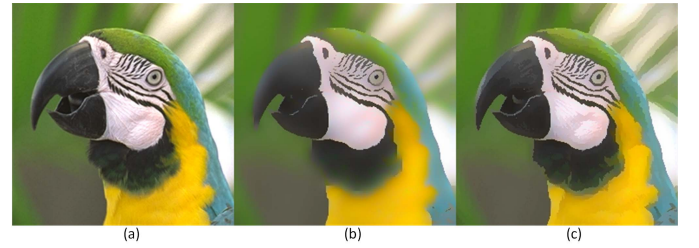


Fig. 4. The effect comparison of positive graph and negative graph on image reconstruction. (a) Input image; (b) Reconstructed image using positive graph; (c) Reconstructed image using negative graph. After a few iterations, positive graph based graph Laplacian smoothness prior tends to oversmoothing, which negative graph based counterpart still preserves large-scale structures well.

words, the nodes are divided into two clusters of same values. In each cluster, edges are only connecting neighboring nodes. We have two kinds of edge weight assignment. The first graph has small positive edge weight 0.1 connecting nodes 6 and 7, while the second graph has negative edge weight -0.01 . The rest of the edges have weight 1. We see that while \mathbf{v}_2 of the positive-only graph is PWS in Fig. 3-(a), \mathbf{v}_1 of the signed graph is PWC in Fig. 3-(b).

Furthermore, in Fig. 4, we provide a comparison result of positive-only graph and signed graph based signal smoothness priors on image reconstruction. We obtain a reconstructed image by solving the following optimization problem:

$$\min_{\mathbf{x}} \|\mathbf{x} - \mathbf{x}_0\|_2^2 + \lambda \mathbf{x}^\top \widehat{\mathbf{L}} \mathbf{x} \quad (6)$$

where \mathbf{x}_0 is the input image *Parrot*, $\widehat{\mathbf{L}}$ is \mathbf{L} or $\mathcal{L} = \mathbf{L} + \Delta$ for positive-only graph and signed graph, respectively. The above optimization is performed iteratively, *i.e.*, in t -th iteration, the last reconstruction \mathbf{x}^{t-1} replaces \mathbf{x}_0 in (6). We observe that after a few iterations, the positive-only graph based smoothness prior tends to oversmooth image structures. In contrast, the signed graph based smoothness prior smooths pixels in the same region but enhances the differences between different regions. This demonstrates the advantage of the constructed signed graph.

C. Robust Edge Weight Estimation

In practice, given a compressed patch, it is difficult to estimate the ground truth gradient $x_i - x_j$ in (3) accurately, resulting in an inappropriate edge weight $w_{i,j}$. We thus

propose to robustly estimate edge weights for graphs of illumination and reflectance pixel patches.

Suppose we are given an initial estimate of illumination / reflectance. The key idea to obtain a robust estimate of edge weights is to treat weights themselves as a signal \mathbf{z} that is smooth with respect to a *dual graph* by assumption [14]. Specifically, as illustrated in Fig. 1-(b), an edge $w_{i,j}$ in the original graph \mathcal{G} becomes a vertex z_k in the dual \mathcal{G}^d and connects to other vertices z_m in \mathcal{G}^d that correspond to edges in \mathcal{G} with one common endpoint with $w_{i,j}$. All links in \mathcal{G}^d have weights equal to 1. Using the resulting graph Laplacian \mathbf{L}^d , we can write a simple optimization objective with a l_2 -norm fidelity term and a GLR prior for edge weight signal \mathbf{z} :

$$\min_{\mathbf{z}} \|\mathbf{z} - \mathbf{w}\|_2^2 + \mu^d \mathbf{z}^\top \mathbf{L}^d \mathbf{z} \quad (7)$$

where \mathbf{w} is the computed edge weight vector from the initial estimate of illumination / reflectance according to (3), and μ^d is a parameter. (7) can be efficiently solved via a system of linear equations:

$$(\mathbf{I} + \mu^d \mathbf{L}^d) \mathbf{z}^* = \mathbf{w} \quad (8)$$

Because the matrix on the left is symmetric, positive definite and sparse, (8) can be solved efficiently using *conjugate gradient* (CG) without matrix inversion [41]. Essentially, assuming that each weight sample z_k is similar to its connected neighbors, (8) performs a low-pass filtering on the weight signal \mathbf{w} for denoising.

D. Negative Edge Weight Selection

Using the above procedure, one can obtain a good initial estimate of positive edge weights for both illumination and reflectance patches. For a reflectance patch, in addition we partition the patch into two and check the difference in intensity value of the respective centroid pixels. If the difference is sufficiently large, we employ the signed graph construction strategy as described in Section IV-B. Unlike a positive edge weight that reflects inter-node similarity, the negative edge weight is used to accentuate the difference in intensity between two connected pixels in a patch. The larger in magnitude the negative edge weight, the bigger the resulting intensity difference for the connected pixel pair, but the less PWC in shape for the first eigenvector of the graph Laplacian. In our experiment, we manually select this negative edge weight to induce a large inter-pixel difference in the reconstructed signal, while keeping the first eigenvector roughly PWC.

E. Optimization Objective

Combining the two image priors for illumination and reflectance and the quantization bin constraint, using our image model in (1) we arrive at our objective function:

$$\begin{aligned} & \min_{\mathbf{l}, \mathbf{r}} \mathbf{l}^\top (\mathbf{L}_l + \alpha \mathbf{L}_l^2) \mathbf{l} + \mu \mathbf{r}^\top \mathcal{L}_r \mathbf{r} \\ & \text{s.t. } \left(\mathbf{q} - \frac{1}{2} \right) \mathbf{Q} \preceq \mathbf{T} \tau \mathbf{l} \odot \mathbf{r} \prec \left(\mathbf{q} + \frac{1}{2} \right) \mathbf{Q} \end{aligned} \quad (9)$$

where \mathbf{L}_l and \mathcal{L}_r are the graph Laplacian and generalized graph Laplacian for the underlying graphs \mathcal{G}_l and \mathcal{G}_r for

Algorithm 1 The Proposed Joint Dequantization and Contrast Enhancement Algorithm

Input: The observed image patch \mathbf{y} , the contrast boosting fact τ^{-1} .

Output: The illumination component \mathbf{l}^* , the texture layer \mathbf{r}^* , and the enhanced patch \mathbf{y}^* .

- 1: map \mathbf{y} from RGB space to HSV space, and only process V-channel \mathbf{v} ;
- 2: Initialize the illumination component $\mathbf{l}^0(i) = \max_{c \in \{R, G, B\}} \mathbf{y}^c(i)$;
- 3: Initialize the reflectance component $\mathbf{r}^0 = \mathbf{v} / \mathbf{l}^0$.

For outer iterations

Procedure 1: Fix \mathbf{l} and optimize \mathbf{r}

- 4: Build a graph on the estimated reflectance in last iteration;
- 5: Build the dual graph and derive the refined edge weights \mathbf{w} by addressing (7);
- 6: Compute the graph Laplacian regularizer \mathcal{L}_r ;
- 7: Estimate the reflectance \mathbf{r} by addressing $\min_{\mathbf{r}} \mu \mathbf{r}^\top \mathcal{L}_r \mathbf{r} + I_C(\mathbf{T} \tau \text{diag}(\mathbf{l}) \mathbf{r})$ using accelerated proximal gradient optimization.

Procedure 2: Fix \mathbf{r} and optimize \mathbf{l}

- 8: Build a graph on the estimated illumination in last iteration;
- 9: Build the dual graph and derive the refined edge weights \mathbf{w} by addressing (7);
- 10: Compute the graph Laplacian regularizer \mathbf{L}_l ;
- 11: Estimate the illumination \mathbf{l} by addressing $\min_{\mathbf{l}} \mathbf{l}^\top (\mathbf{L}_l + \alpha \mathbf{L}_l^2) \mathbf{l} + I_C(\mathbf{T} \tau \text{diag}(\mathbf{r}) \mathbf{l})$ using accelerated proximal gradient optimization.

End

- 12: Compute the enhance V-channel $\mathbf{v}^* = \mathbf{l}^* \cdot \mathbf{r}^*$.

- 13: Convert HSV to RGB to get the enhanced patch as \mathbf{y}^* ;
-

illumination and reflectance pixel patches respectively; μ is a parameter to trade off the two priors; \mathbf{q} is the vector of quantized transform coefficients corresponding to block $\tau \mathbf{l} \odot \mathbf{r}$, and \mathbf{Q} the vector of corresponding QPs.

For the estimation of contrast reduction factor τ , we extend the pixel-wise approach in OCTM [3] to the patch-wise approach. Specifically, for each patch \mathbf{y} , we compute its average gray level m , which is more robust to noise than the gray level of a single pixel. Then we get the optimal enhanced gray level $T(m)$ according to OCTM [3], and then derive the contrast boost factor $\tau^{-1} = T(m)/m$.

We summarize the algorithm flow in Algorithm I.

V. OPTIMIZATION ALGORITHM

A. Unconstrained Problem Definition

Instead of addressing the constrained problem in (9), we first convert it to an unconstrained version as follow. First, we define a convex set $\mathcal{C} \triangleq \{\mathbf{y} \mid (\mathbf{q} - \frac{1}{2}) \mathbf{Q} \preceq \mathbf{y} \prec (\mathbf{q} + \frac{1}{2}) \mathbf{Q}\}$. We then define an indicator function $I_C(\mathbf{y})$ as follow:

$$I_C(\mathbf{y}) = \begin{cases} 0 & \text{if } \mathbf{y} \in \mathcal{C} \\ \infty & \text{o.w.} \end{cases} \quad (10)$$

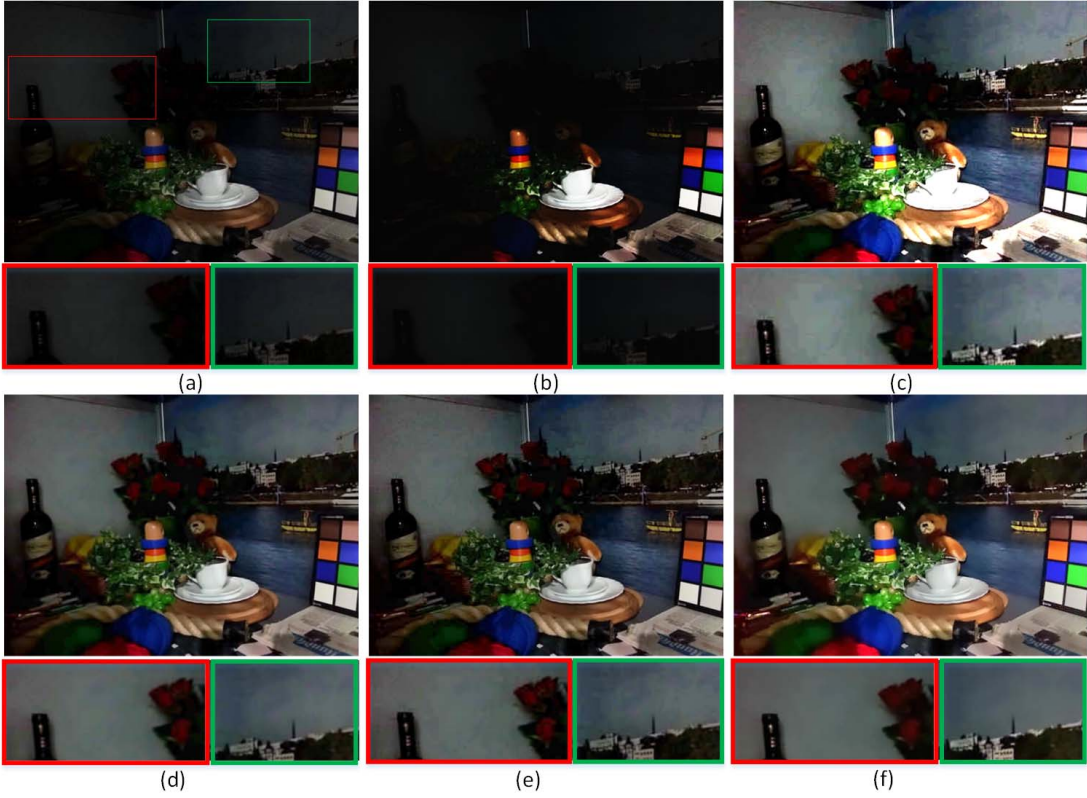


Fig. 5. Visual comparison of different image enhancement methods on *Bear*. (a) Input image; (b) Li's method [20]; (c) LIME [5] + SA-DCT [9]; (d) ANCE [7] + WVM [4]; (e) WVM [4] + ANCE [7]; (f) Graph Retinex.

We can now rewrite (9) into its unconstrained version using $I_C(\mathbf{y})$:

$$\min_{\mathbf{l}, \mathbf{r}} \mathbf{l}^\top (\mathbf{L}_l + \alpha \mathbf{L}_l^2) \mathbf{l} + \mu \mathbf{r}^\top \mathcal{L}_r \mathbf{r} + I_C(\mathbf{T}\tau \mathbf{l} \odot \mathbf{r}) \quad (11)$$

B. Initialization

In practical implementation, we map the RGB color test images into the HSV (Hue, Saturation and Value) color space and only process the V-channel, and then map back to the RGB domain. Define \mathbf{v} as the V-channel component of the input patch \mathbf{y} . To obtain the initial illumination, we extend the idea of Land's another pioneer work on Retinex theory [42] and estimate the initial \mathbf{l}^0 by seeking the maximum value of three RGB color channels on each pixel i :

$$\mathbf{l}^0(i) = \max_{c \in \{R, G, B\}} \mathbf{y}^c(i) \quad (12)$$

Then we derive initial reflectance \mathbf{r}^0 according to the image formation model: $\mathbf{r}^0 = \mathbf{v} ./ \mathbf{l}^0$.

C. Accelerated Proximal Gradient Optimization

We employ an alternating approach to solve (11), where we fix one variable and optimize the other and vice versa. Specifically, when \mathbf{l} is fixed, we seek the optimal \mathbf{r} by solving the following:

$$\min_{\mathbf{r}} \mu \mathbf{r}^\top \mathcal{L}_r \mathbf{r} + I_C(\mathbf{T}\tau \text{diag}(\mathbf{l})\mathbf{r}) \quad (13)$$

where the first term is convex and differentiable, but the second term is convex but non-differentiable. We thus use APG to solve (13), where the proximal mapping for an indicator function of a convex set is just an Euclidean projection:

$$\text{prox}_{I_C}(\mathbf{y}) = P_C(\mathbf{y}) \quad (14)$$

Because convex set C is a high-dimensional box in the DCT domain, projection is simple clipping of each entry (DCT coefficient) y_i to within range $[(q_i - \frac{1}{2})Q_i, (q_i + \frac{1}{2})Q_i]$.

To simplify the argument of the proximal mapping, we first define DCT coefficients $\boldsymbol{\kappa}$:

$$\boldsymbol{\kappa} = \mathbf{T}\tau \text{diag}(\mathbf{l})\mathbf{r} \quad (15)$$

and \mathbf{r} can be recovered from $\boldsymbol{\kappa}$ easily since DCT transform \mathbf{T} is invertible:

$$\mathbf{r} = \frac{1}{\tau} \text{diag}^{-1}(\mathbf{l}) \mathbf{T}^{-1} \boldsymbol{\kappa}. \quad (16)$$

We can thus rewrite (13) as:

$$\begin{aligned} \min_{\boldsymbol{\kappa}} \frac{\mu}{\tau^2} \boldsymbol{\kappa}^\top \underbrace{\left(\mathbf{T}^{-1} \right)^T \text{diag}^{-1}(\mathbf{l}) \mathcal{L}_r \text{diag}^{-1}(\mathbf{l}) \mathbf{T}^{-1} \boldsymbol{\kappa}}_{\mathbf{P}_r} + I_C(\boldsymbol{\kappa}) \\ = \frac{\mu}{\tau^2} \boldsymbol{\kappa}^\top \mathbf{P}_r \boldsymbol{\kappa} + I_C(\boldsymbol{\kappa}) \end{aligned} \quad (17)$$

To adopt an APG approach, we first define (with initial point $\boldsymbol{\kappa}^{(0)} = \boldsymbol{\kappa}^{(-1)}$):

$$\boldsymbol{\kappa}^{(k-1)} = \boldsymbol{\kappa}^{(k-1)} + \frac{k-2}{k+1} (\boldsymbol{\kappa}^{(k-1)} - \boldsymbol{\kappa}^{(k-2)}) \quad (18)$$



Fig. 6. Visual comparison of different image enhancement methods on *Riverside*. (a) Input image; (b) Li's method [20]; (c) LIME [5] + SA-DCT [9]; (d) ANCE [7] + WVM [4]; (e) WVM [4] + ANCE [7]; (f) Graph Retinex.

where $\mathbf{v}^{(k-1)}$ is an *extrapolated* point computed from the two previous solutions $\boldsymbol{\kappa}^{(k-1)}$ and $\boldsymbol{\kappa}^{(k-2)}$.

We now compute the proximal gradient procedure using $\mathbf{v}^{(k-1)}$ as follow:

$$\boldsymbol{\kappa}^{(k)} = P_C(\mathbf{v}^{(k-1)} - t \left(\frac{2\mu}{\tau^2} \right) \mathbf{P}_r \mathbf{v}^{(k-1)}) \quad (19)$$

where t is a step size. The APG algorithm has convergence rate $O(1/k^2)$, which is the fastest possible for first-order methods. As discussed, we can recover $\mathbf{r}^{(k)}$ from $\boldsymbol{\kappa}^{(k)}$ easily using (16).

Since the proximal mapping in our case is simple DCT coefficient clipping, which is very computation-efficient, we can implement *backtracking line search* also for additional speedup. Specifically, let $t_0 = 1$ and fix $\beta < 1$. At each iteration k , initialize $t = t_{k-1}$ and compute $\boldsymbol{\kappa}^* = \boldsymbol{\kappa}^{(k)}$ using (19), then while:

$$\begin{aligned} \frac{\mu}{\tau^2} \boldsymbol{\kappa}^* \mathbf{P}_r \boldsymbol{\kappa}^* &> \frac{\mu}{\tau^2} \mathbf{v}^{(k-1)} \mathbf{P}_r \mathbf{v}^{(k-1)} + \frac{2\mu}{\tau^2} \mathbf{P}_r (\boldsymbol{\kappa}^* - \mathbf{v}^{(k-1)}) \\ &\quad + \frac{1}{2t} \|\boldsymbol{\kappa}^* - \mathbf{v}^{(k-1)}\|_2^2 \end{aligned} \quad (20)$$

compute $t := \beta t$, and update $\boldsymbol{\kappa}^*$ using (19) with new t .

Similarly, when \mathbf{r} is fixed, we seek the optimal \mathbf{l} as follow:

$$\min_{\mathbf{l}} \mathbf{l}^\top (\mathbf{L}_l + \alpha \mathbf{L}_l^2) \mathbf{l} + I_C(\mathbf{T}\tau \operatorname{diag}(\mathbf{r})\mathbf{l}) \quad (21)$$

With a similar change of variables $\mathbf{l} = \frac{1}{\tau} \operatorname{diag}^{-1}(\mathbf{r}) \mathbf{T}^{-1} \boldsymbol{\eta}$, we can rewrite the objective (21) as:

$$\begin{aligned} \min_{\boldsymbol{\eta}} \frac{1}{\tau^2} \boldsymbol{\eta}^\top & \underbrace{\left(\mathbf{T}^{-1} \right)^\top \operatorname{diag}^{-1}(\mathbf{r}) \left(\mathbf{L}_l + \alpha \mathbf{L}_l^2 \right) \operatorname{diag}^{-1}(\mathbf{r}) \mathbf{T}^{-1} \boldsymbol{\eta}}_{\mathbf{Q}_l} \\ & + I_C(\boldsymbol{\eta}) \\ &= \frac{1}{\tau^2} \boldsymbol{\eta}^\top \mathbf{Q}_l \boldsymbol{\eta} + I_C(\boldsymbol{\eta}) \end{aligned} \quad (22)$$

We first similarly define an extrapolated point $\mathbf{u}^{(k-1)}$ (with initial point $\boldsymbol{\eta}^{(0)} = \boldsymbol{\eta}^{(-1)}$):

$$\mathbf{u}^{(k-1)} = \boldsymbol{\eta}^{(k-1)} + \frac{k-2}{k+1} (\boldsymbol{\eta}^{(k-1)} - \boldsymbol{\eta}^{(k-2)}) \quad (23)$$

The resulting proximal gradient procedure is similar:

$$\boldsymbol{\eta}^{(k)} = P_C(\mathbf{u}^{(k-1)} - t \left(\frac{2}{\tau^2} \right) \mathbf{Q}_l \mathbf{u}^{(k-1)}) \quad (24)$$

where t is a step size. Similar backtracking line search can be performed for $\boldsymbol{\eta}^{(k)}$ also.

After a few iterations (two iterations in practical implementation), we derive the locally optimal estimates \mathbf{l}^* and \mathbf{r}^* corresponding to illumination and reflectance respectively. The recovered patch is obtained as $\mathbf{v}^* = \mathbf{l}^* \cdot \mathbf{r}^*$. Finally, the updated

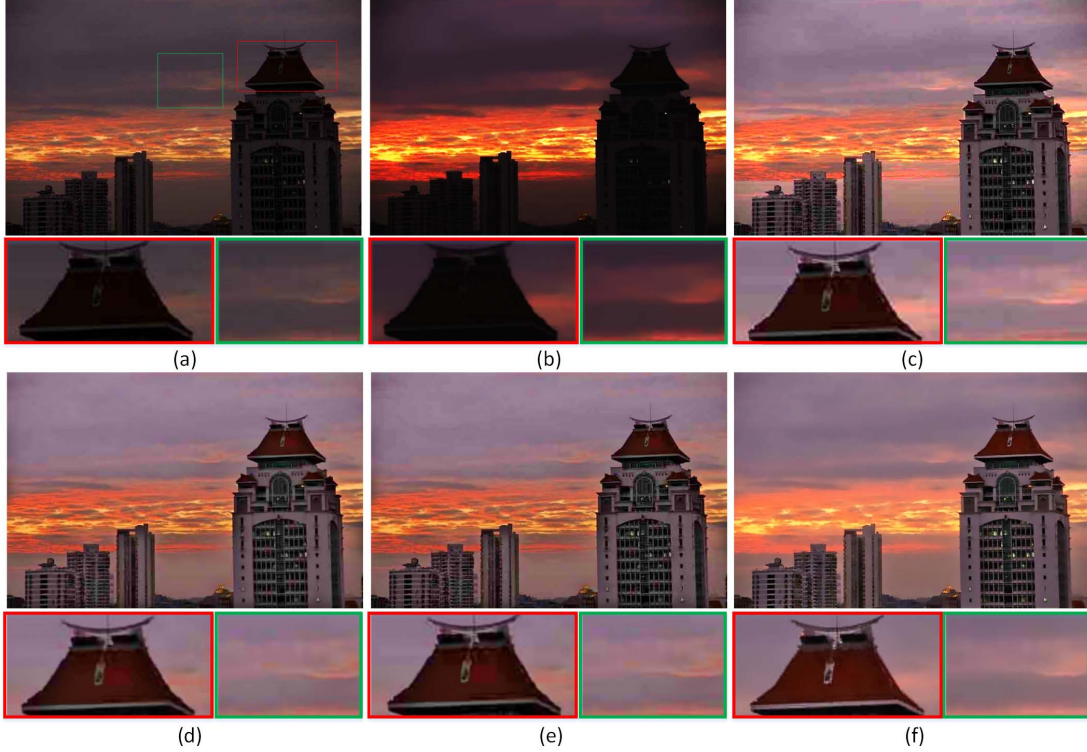


Fig. 7. Visual comparison of different image enhancement methods on *Nightfall*. (a) Input image; (b) Li's method [20]; (c) LIME [5] + SA-DCT [9]; (d) ANCE [7] + WVM [4]; (e) WVM [4] + ANCE [7]; (f) Graph Retinex.

HSV image is mapped back to RGB color space to obtain the enhanced image.

VI. EXPERIMENTATION

In this section, we offer comprehensive evaluation of the performance of our proposed algorithm compared with four state-of-the-art methods, including: 1) Li's method [20], which to the best of our knowledge, is the only work that considers joint contrast enhancement and JPEG artifact suppression; 2) LIME [5], a recent weighted-TV based Retinex scheme, whose results are *post-processed* using a state-of-the-art deblocking algorithm SA-DCT [9] to remove blocking artifacts; 3) weighted variational model (WVM) based Retinex [4], which are examined with two modes:

- **ANCE+WVM:**

The input JPEG images are first *pre-processed* by another state-of-the-art compression artifact reduction algorithm ANCE [7] to remove compression artifacts, then enhanced by WVM.

- **WVM+ANCE:**

The input JPEG images are first enhanced by WVM, then *post-processed* by ANCE to remove compression artifacts.

All source codes are provided by their authors, which are run with the tuned parameter settings that generate the best results for fair comparison.

To demonstrate the effectiveness of our algorithm, we test eight images including natural scenes with various low-light conditions, which are collected from the test set of [5] and

Multi-Exposure Fusion Image Database [43]. Considering most JPEG images are compressed using quality factor (QF) ranging from 70 to 90 (such as images in Facebook), we show the results when $QF = 70$. In our scheme, we fixed $\mu = 0.05$ for the following tests.

A. Subjective Quality Comparison

The goal of our work is to design an algorithm that enhances the contrast of low-lighting images while suppressing JPEG compression artifacts. In this subsection, we provide subjective quality comparison to show the superiority of our algorithm.

Fig. 5 shows the results of the five methods for an indoor image *Bear* with poor lighting conditions, which contains smooth areas such as the wall and texture regions such as the flower, the bear and the green plant. We observe that Li's method in (b) failed to enhance the whole image well, making the dark regions even darker while bright regions even brighter. The LIME algorithm followed by SA-DCT for deblocking in (c) still has strong compression artifacts, especially in the wall areas. The reason is that LIME has over-enhancement effect (such as the teacup), which also amplifies the coding artifacts, making the subsequent deblocking algorithm SA-DCT difficult to remove blocking artifacts. The pre-processing strategy, ANCE + WVM in (d), works better than the post-processing strategy WVM + ANCE shown in (e), in which some blocking artifacts are removed before enhancement. Our proposed Graph Retinex achieved high contrast and small distortion at the same time. It is clear to see that our proposal in (f) suppressed blocking artifacts much better than



Fig. 8. Visual comparison of different image enhancement methods on *Man*. (a) Input image; (b) Li's method [20]; (c) LIME [5] + SA-DCT [9]; (d) ANCE [7] + WVM [4]; (e) WVM [4] + ANCE [7]; (f) Graph Retinex.

other methods, while the enhancement also performs well for the whole image. There is no adverse over-enhancement effect.

Fig. 6 shows the results of compared methods for an outdoor image *Riverside* with non-uniform light at night. Again, our proposed Graph Retinex achieved the best subjective quality. It is clear that Graph Rextinex was more robust to noise than the other four state-of-the-art methods.

Fig. 7 shows results for the test image *Nightfall* that contains buildings and sky. In (b), Li's method removed blocking artifacts due to JPEG compression well, but failed to boost the contrast of the whole image. The post-processing strategy, including LIME + SA-DCT in (c) and WVM + ANCE in (e), improved the brightness level of the whole picture, but also amplified compression noise in the image. In (c) and (e), the blocking artifacts became more visible, especially in the sky areas. The pre-processing strategy, *i.e.*, ANCE + WVM in (d), produced better visual result than the post-processing strategy. It is clear to see that our proposal in (f) suppressed blocking artifacts much better than other methods.

In Fig. 8, results for an indoor image *Man* are presented. The human face is obviously the salient area. The result of LIME + SA-DCT in (c) has strong blocking artifacts on the human face. The pre- and post-processing strategies of ANCE + WVM and WVM + ANCE in (d) and (e) work better than LIME + SA-DCT, but still cannot produce satisfactory results. In contrast, our proposal in (f) generated a much clearer

face; the contrast is boosted appropriately, and compression noises are suppressed well. It should be noted that, although our method produces much better enhanced visual result in the face region, it leads to somewhat over-smoothing in the background region.

In Fig. 9, results for an outdoor image *Tower* are shown. It can be observed that the proposed Graph Retinex removed most blocking artifacts in the grass while boosting the details of the sky.

Comparison of the remaining three test images are shown in Fig. 10, Fig. 11, and Fig. 12. It can be observed that the results generated by our algorithm have less compression artifacts and better boosting effects.

It is worth noting that, recently there are three objective image quality measures for evaluating performance of dequantization, *i.e.*, BPRI [44], BMPRI [45] and UCA [46]. In this paper, we consider both dequantization and contrast enhancement. For contrast enhancement, it is difficult to know which is the ideal case, and thus we cannot generate pseudo reference image like the mentioned methods. Therefore, these metrics are not suitable for objective quality evaluation in this paper.

B. Subjective Testing

We also conducted a subjective test to verify the performance of our method compared to other ones based

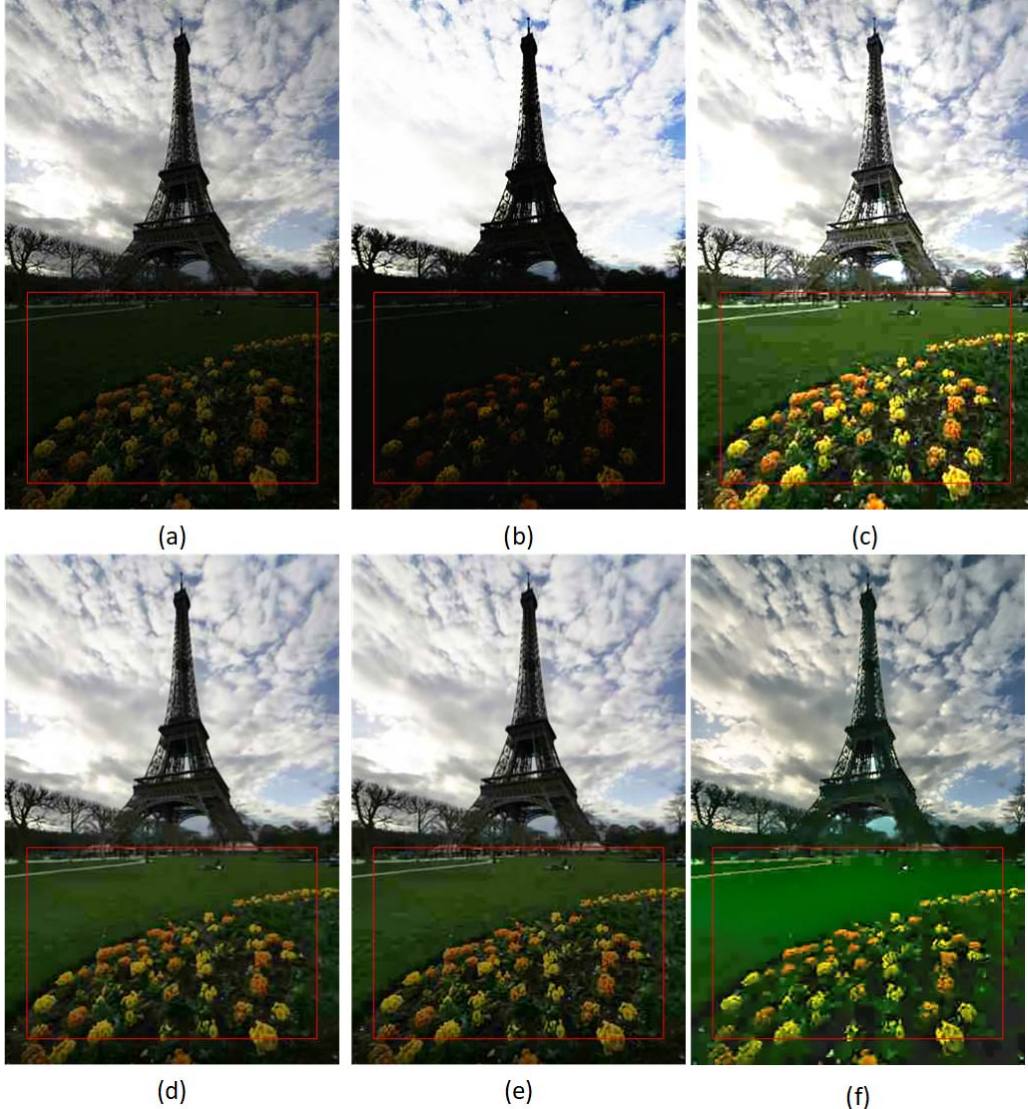


Fig. 9. Visual comparison of different image enhancement methods on *Tower*. (a) Input image; (b) Li's method [20]; (c) LIME [5] + SA-DCT [9]; (d) ANCE [7] + WVM [4]; (e) WVM [4] + ANCE [7]; (f) Graph Retinex.

on a two-alternative forced choice (2AFC) process, which is widely used in psychophysical studies. Eight test images are selected for testing. 40 participants with age 18 to 41 and with normal or corrected to normal vision were invited to take this test. Participants were familiarized with the testing procedure before the start of the experiment. In each trial, a participant was shown side-by-side a pair of images: enhanced results of the same image by the proposed Graph Retinex method and one of four compared methods, and was asked (forced) to choose the one he/she believed to have better image quality. In the 2AFC test, the side-by-side comparison was randomly slotted into four test sequences, where for each sequence, the ordering of the ten test image pairs was also randomized. Each image pair was shown on a 8-bit 27" monitor with contrast and bright set at 75%. The distance from the subject to the monitor is approximately twice the monitor's height (335.7mm). The illumination of the room was in the 300-320 Lux range. Participants observed each

image pair for 10 seconds, and entered the score in the next 5 seconds. This testing procedure followed closely guidelines provided by ITU-R BT.500 [47].

The vote statistics of participants are shown in Table I. We see that for all test images, the participants selected our proposed Graph Retinex over competing schemes by a clear margin. This validates the superior visual quality of our method over competing schemes. Moreover, we used the two-sided chi-square χ^2 test [48] to examine the statistical significance of the results. The null hypothesis is that there is no preference for each pair of images. Under this hypothesis, the expected number of votes should be equal. As a rule of thumb in experimental sciences, the null hypothesis is accepted when $p \gg 0.05$. From Table I, we see that for all test images, the p -value [48] of χ^2 is smaller than 0.05, most of which are significantly smaller. We can thus conclude that statistically participants showed significant preference for our method.

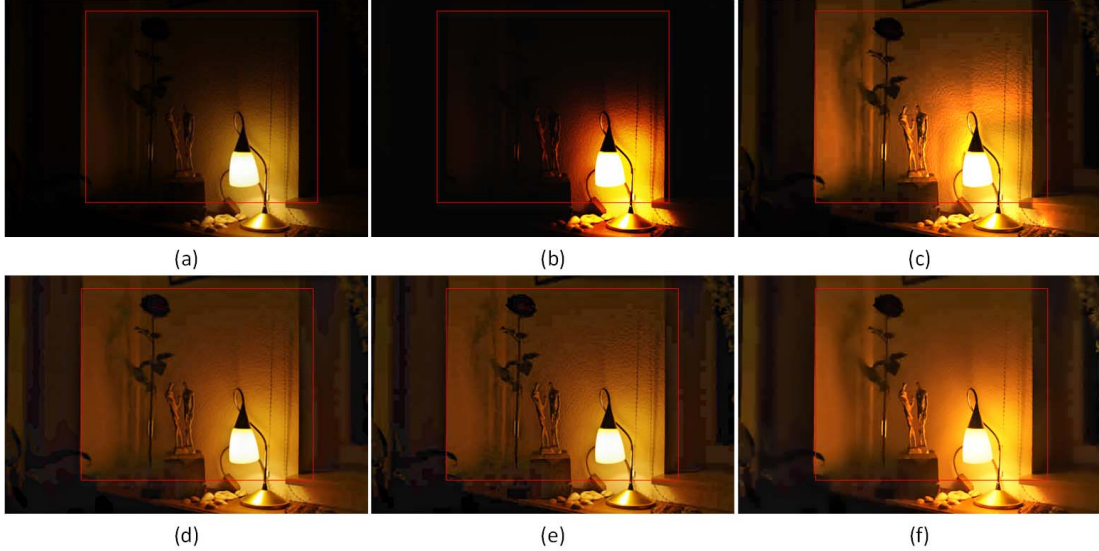


Fig. 10. Visual comparison of different image enhancement methods on *Lamp*. (a) Input image; (b) Li's method [20]; (c) LIME [5] + SA-DCT [9]; (d) ANCE [7] + WVM [4]; (e) WVM [4] + ANCE [7]; (f) Graph Retinex.

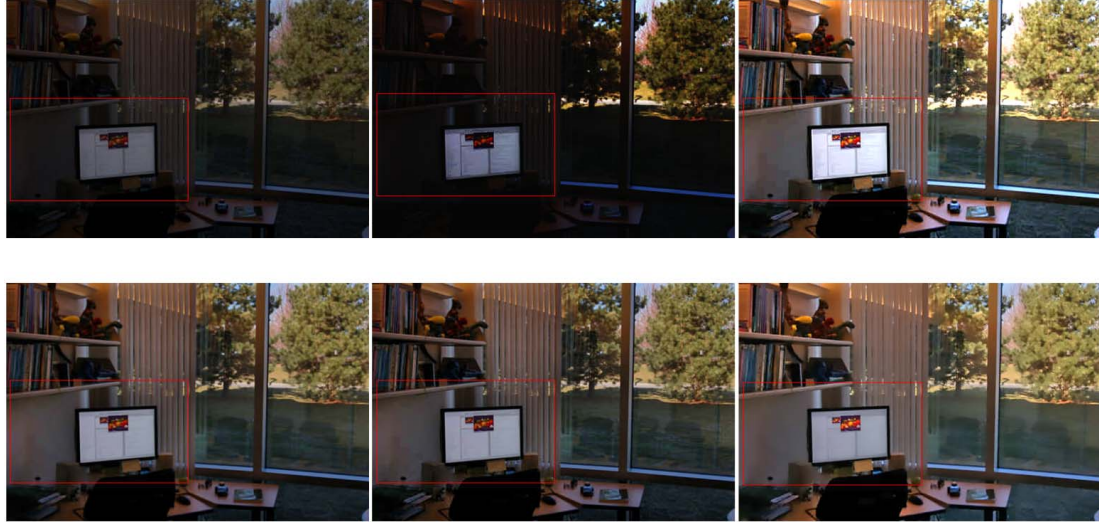


Fig. 11. Visual comparison of different image enhancement methods on *Office*. (a) Input image; (b) Li's method [20]; (c) LIME [5] + SA-DCT [9]; (d) ANCE [7] + WVM [4]; (e) WVM [4] + ANCE [7]; (f) Graph Retinex.

TABLE I
SUBJECTIVE EVALUATION OF COMPARED METHODS. EACH TABLE CELL SHOWS THE VOTE STATISTICS
AND THE CORRESPONDING p -VALUE OF TWO-SIDED χ^2 TEST

	<i>Bear</i>	<i>Nightfall</i>	<i>Riverside</i>	<i>Man</i>	<i>Lamp</i>	<i>Office</i>	<i>Tower</i>	<i>Moonlight</i>
Graph Retinex:Li's method p -value	40:0 2.5396e-10							
Graph Retinex:LIME + SA-DCT p -value	38:2 1.2549e-08	37:3 7.6213e-08	38:2 1.2549e-08	35:5 2.1014e-06	36:4 4.2004e-07	30:10 0.0016	33:7 3.9402e-05	28:12 0.0114
Graph Retinex:ANCE + WVM p -value	27:13 0.0269	35:5 2.1014e-06	36:4 4.2004e-07	35:5 2.1014e-06	27:13 0.0269	28:12 0.0114	32:8 1.4780e-04	29:11 0.0044
Graph Retinex:WVM + ANCE p -value	37:3 7.6213e-08	38:2 1.2549e-08	38:2 1.2549e-08	37:3 7.6213e-08	33:7 3.9402e-05	29:11 0.0044	36:4 4.2004e-07	30:10 0.0016

C. Complexity Comparison

We also provide computational complexity comparison. The compared methods are running on a typical laptop computer (Intel Core i7 CPU 2.9GHz, 16G Memory, Win10,

Matlab R2016a). As depicted in Table II, the complexity of our method is lower than Li's method, which is also a unified algorithm considering both contrast enhancement and compression artifact suppression. It is also much lower

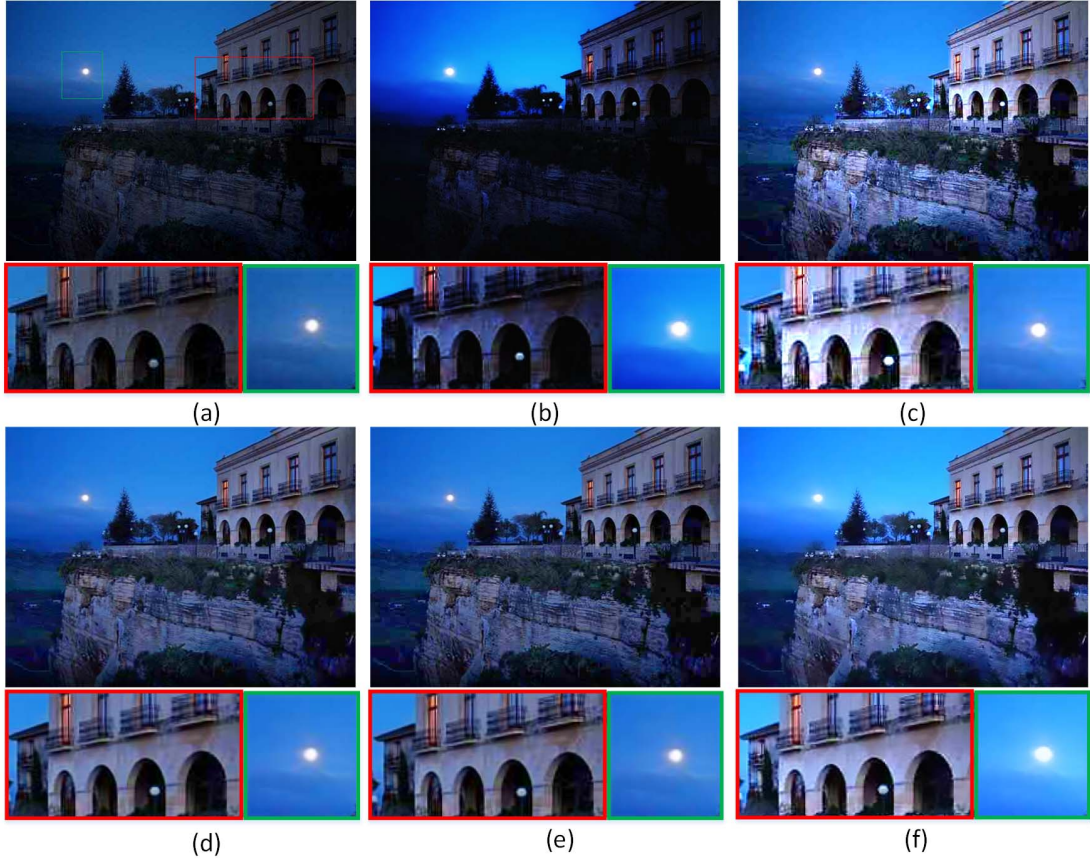


Fig. 12. Visual comparison of different image enhancement methods on *Moonlight*. (a) Input image; (b) Li's method [20]; (c) LIME [5] + SA-DCT [9]; (d) ANCE [7] + WVM [4]; (e) WVM [4] + ANCE [7]; (f) Graph Retinex.

TABLE II
COMPLEXITY COMPARISON WITH RESPECT TO RUNNING TIME (s)

Image	Resolution	Li's method	LIME + SA-DCT	ANCE + WVM	WVM + ANCE	Our method
<i>Bear</i>	490 × 365	20.22	12.80	241.23	241.10	9.40
<i>Nightfall</i>	690 × 460	35.11	13.73	438.23	428.47	20.40
<i>Riverside</i>	720 × 680	56.09	14.26	618.56	617.99	24.22
<i>Man</i>	896 × 592	63.50	15.87	681.56	683.51	27.40
<i>Lamp</i>	512 × 342	20.48	11.55	223.47	224.59	9.12
<i>Office</i>	512 × 340	17.22	11.48	224.13	226.93	9.48
<i>Tower</i>	341 × 512	16.32	11.48	232.66	229.83	9.58
<i>Moonlight</i>	490 × 365	27.69	11.98	310.05	316.59	12.81
Average		27.34	12.41	328.60	327.11	14.80

than the pre-processing strategy ANCE + WVM and the post-processing strategy WVM + ANCE. The running time of our method is comparable with LIME + SA-DCT. Please note that the main routines of SA-DCT are written in C.

VII. CONCLUSION

To restore images captured in poorly lit environments that suffer from both JPEG compression artifacts and low contrast, we propose a graph-based joint dequantization / contrast enhancement scheme. The key idea is to decompose the target image into a product of illumination and reflectance components via Retinex theory, where each component can be

mathematically described as a signal smoothness prior on an appropriately defined graph. Specifically, we use signed graphs where positive edges connect similar pixels for averaging to combat noise, and negative edges connect dissimilar pixels to accentuate their differences for enhancement. Experimental results show cleaner and higher-contrast images compared to state-of-the-art methods.

There are some limitations to our current work. First, the determination of positive and negative edge weights is tuned manually and thus not optimal in any sense. Second, the connectivity of the graph used (4-connected graph, where each pixel is connected to its four nearest neighbors)

is not optimized. While our hand-tuned parameters and connectivity led to good visual performance in our experiments, we plan to study these issues more theoretically as future work.

REFERENCES

- [1] R. Kimmel, M. Elad, D. Shaked, R. Keshet, and I. Sobel, "A variational framework for Retinex," *Int. J. Comput. Vis.*, vol. 52, no. 1, pp. 7–23, 2003.
- [2] M. K. Ng and W. Wang, "A total variation model for Retinex," *SIAM J. Imag. Sci.*, vol. 4, no. 1, pp. 345–365, 2011.
- [3] X. Wu, "A linear programming approach for optimal contrast-tone mapping," *IEEE Trans. Image Process.*, vol. 20, no. 5, pp. 1262–1272, May 2011.
- [4] X. Fu, D. Zeng, Y. Huang, X.-P. Zhang, and X. Ding, "A weighted variational model for simultaneous reflectance and illumination estimation," in *Proc. CVPR*, Jun. 2016, pp. 2782–2790.
- [5] X. Guo, Y. Li, and H. Ling, "LIME: Low-light image enhancement via illumination map estimation," *IEEE Trans. Image Process.*, vol. 26, no. 2, pp. 982–993, Feb. 2017.
- [6] G. K. Wallace, "The JPEG still picture compression standard," *IEEE Trans. Consum. Electron.*, vol. 38, no. 1, pp. 18–34, Feb. 1992.
- [7] X. Zhang, R. Xiong, X. Fan, S. Ma, and W. Gao, "Compression artifact reduction by overlapped-block transform coefficient estimation with block similarity," *IEEE Trans. Image Process.*, vol. 22, no. 12, pp. 4613–4626, Dec. 2013.
- [8] X. Liu, G. Cheung, X. Wu, and D. Zhao, "Random walk graph Laplacian-based smoothness prior for soft decoding of JPEG images," *IEEE Trans. Image Process.*, vol. 26, no. 2, pp. 509–524, Feb. 2017.
- [9] A. Foi, V. Katkovnik, and K. Egiazarian, "Pointwise shape-adaptive DCT for high-quality denoising and deblocking of grayscale and color images," *IEEE Trans. Image Process.*, vol. 16, no. 5, pp. 1395–1411, May 2007.
- [10] D. I. Shuman, S. K. Narang, P. Frossard, A. Ortega, and P. Vandergheynst, "The emerging field of signal processing on graphs: Extending high-dimensional data analysis to networks and other irregular domains," *IEEE Signal Process. Mag.*, vol. 30, no. 3, pp. 83–98, May 2013.
- [11] G. Cheung, E. Magli, Y. Tanaka, and M. K. Ng, "Graph spectral image processing," *Proc. IEEE*, vol. 106, no. 5, pp. 907–930, May 2018.
- [12] K. Bredies and M. Holler, "A TGV-based framework for variational image decompression, zooming, and reconstruction. Part I: Analytics," *SIAM J. Imag. Sci.*, vol. 8, no. 4, pp. 2814–2850, 2015.
- [13] J. Kunegis, S. Schmidt, A. Lommatzsch, J. Lerner, E. W. De Luca, and S. Alpayrak, "Spectral analysis of signed graphs for clustering, prediction and visualization," in *Proc. SIAM ICDM*, 2010, pp. 559–570.
- [14] W. Hu, G. Cheung, and M. Kazui, "Graph-based dequantization of block-compressed piecewise smooth images," *IEEE Signal Process. Lett.*, vol. 23, no. 2, pp. 242–246, Feb. 2016.
- [15] H. Yue, J. Yang, X. Sun, F. Wu, and C. Hou, "Contrast enhancement based on intrinsic image decomposition," *IEEE Trans. Image Process.*, vol. 26, no. 8, pp. 3981–3994, Aug. 2017.
- [16] N. Parikh and S. Boyd, "Proximal algorithms," *Found. Trends Optim.*, vol. 1, no. 3, pp. 127–239, Jan. 2014, doi: [10.1561/2400000003](https://doi.org/10.1561/2400000003).
- [17] D. Zosso, G. Tran, and S. J. Osher, "Non-local Retinex—A unifying framework and beyond," *SIAM J. Imag. Sci.*, vol. 8, no. 2, pp. 787–826, 2015.
- [18] D. J. Jobson, Z.-U. Rahman, and G. A. Woodell, "Properties and performance of a center/surround Retinex," *IEEE Trans. Image Process.*, vol. 6, no. 3, pp. 451–462, Mar. 1997.
- [19] D. J. Jobson, Z.-U. Rahman, and G. A. Woodell, "A multiscale Retinex for bridging the gap between color images and the human observation of scenes," *IEEE Trans. Image Process.*, vol. 6, no. 7, pp. 965–976, Jul. 1997.
- [20] Y. Li, F. Guo, R. T. Tan, and M. S. Brown, "A contrast enhancement framework with JPEG artifacts suppression," in *Proc. Eur. Conf. Comput. Vis.*, 2014, pp. 174–188.
- [21] X. Liu, X. Wu, J. Zhou, and D. Zhao, "Data-driven soft decoding of compressed images in dual transform-pixel domain," *IEEE Trans. Image Process.*, vol. 25, no. 4, pp. 1649–1659, Apr. 2016.
- [22] X. Liu, G. Cheung, C. Lin, D. Zhao, and W. Gao, "Prior-based quantization bin matching for cloud storage of JPEG images," *IEEE Trans. Image Process.*, vol. 27, no. 7, pp. 3222–3235, Jul. 2018.
- [23] G. Zhai, W. Zhang, X. Yang, W. Lin, and Y. Xu, "Efficient image deblocking based on postfiltering in shifted windows," *IEEE Trans. Circuits Syst. Video Technol.*, vol. 18, no. 1, pp. 122–126, Jan. 2008.
- [24] F. Alter, S. Durand, and J. Froment, "Adapted total variation for artifact free decompression of JPEG images," *J. Math. Imag. Vis.*, vol. 23, no. 2, pp. 199–211, 2005.
- [25] X. Liu, X. Wu, J. Zhou, and D. Zhao, "Data-driven sparsity-based restoration of JPEG-compressed images in dual transform-pixel domain," in *Proc. IEEE Conf. CVPR*, Jun. 2015, pp. 5171–5178.
- [26] W. Hu, G. Cheung, A. Ortega, and O. Au, "Multi-resolution graph Fourier transform for compression of piecewise smooth images," *IEEE Trans. Image Process.*, vol. 24, no. 1, pp. 419–433, Jan. 2015.
- [27] W. Hu, G. Cheung, and A. Ortega, "Intra-prediction and generalized graph Fourier transform for image coding," *IEEE Signal Process. Lett.*, vol. 22, no. 11, pp. 1913–1917, Nov. 2015.
- [28] J. Pang and G. Cheung, "Graph Laplacian regularization for image denoising: Analysis in the continuous domain," *IEEE Trans. Image Process.*, vol. 26, no. 4, pp. 1770–1785, Apr. 2017.
- [29] C. Tomasi and R. Manduchi, "Bilateral filtering for gray and color images," in *Proc. 6th IEEE Int. Conf. Comput. Vis.*, Bombay, India, Jan. 1998, pp. 839–846.
- [30] X. Liu, D. Zhai, D. Zhao, G. Zhai, and W. Gao, "Progressive image denoising through hybrid graph Laplacian regularization: A unified framework," *IEEE Trans. Image Process.*, vol. 23, no. 4, pp. 1491–1503, Apr. 2014.
- [31] X. Liu, D. Zhai, R. Chen, X. Ji, D. Zhao, and W. Gao, "Depth super-resolution via joint color-guided internal and external regularizations," *IEEE Trans. Image Process.*, to be published, doi: [10.1109/TIP.2018.2875506](https://doi.org/10.1109/TIP.2018.2875506).
- [32] D. Zhai, X. Liu, X. Ji, D. Zhao, S. Satoh, and W. Gao, "Supervised distributed hashing for large-scale multimedia retrieval," *IEEE Trans. Multimedia*, vol. 20, no. 3, pp. 675–686, Mar. 2018.
- [33] D. Zhai et al., "Parametric local multiview Hamming distance metric learning," *Pattern Recognit.*, vol. 75, pp. 250–262, Mar. 2018.
- [34] M. Elad, *Retinex by Two Bilateral Filters*. Berlin, Germany: Springer, 2005, pp. 217–229, doi: [10.1007/11408031_19](https://doi.org/10.1007/11408031_19).
- [35] D. Zelazo and M. Bürger, "On the definiteness of the weighted Laplacian and its connection to effective resistance," in *Proc. IEEE CDC*, Dec. 2014, pp. 2895–2900.
- [36] Y. Chen, S. Z. Khong, and T. T. Georgiou, "On the definiteness of graph Laplacians with negative weights: Geometrical and passivity-based approaches," in *Proc. Amer. Control Conf.*, Boston, MA, USA, Jul. 2016, pp. 2488–2493.
- [37] L. Chu, Z. Wang, J. Pei, J. Wang, Z. Zhao, and E. Chen, "Finding gangs in war from signed networks," in *Proc. ACM SIGKDD*, 2016, pp. 1505–1514.
- [38] F. Dorfler and F. Bullo, "Kron reduction of graphs with applications to electrical networks," *IEEE Trans. Circuits Syst. I, Reg. Papers*, vol. 60, no. 1, pp. 150–163, Jan. 2013.
- [39] G. Cheung, W.-T. Su, Y. Mao, and C.-W. Lin, "Robust semisupervised graph classifier learning with negative edge weights," *IEEE Trans. Signal Inf. Process. Over Netw.*, vol. 4, no. 4, pp. 712–726, Dec. 2018.
- [40] E. V. Haynsworth and A. M. Ostrowski, "On the inertia of some classes of partitioned matrices," *Linear Algebra Appl.*, vol. 1, no. 2, pp. 299–316, 1968.
- [41] S. Boyd and L. Vandenberghe, *Convex Optimization*. Cambridge, U.K.: Cambridge Univ. Press, 2004.
- [42] E. H. Land, "The Retinex theory of color vision," *Sci. Amer.*, vol. 237, no. 6, pp. 108–128, Dec. 1977.
- [43] K. Ma, K. Zeng, and Z. Wang, "Perceptual quality assessment for multi-exposure image fusion," *IEEE Trans. Image Process.*, vol. 24, no. 11, pp. 3345–3356, Nov. 2015.
- [44] X. Min, K. Gu, G. Zhai, J. Liu, X. Yang, and C. W. Chen, "Blind quality assessment based on pseudo-reference image," *IEEE Trans. Multimedia*, vol. 20, no. 8, pp. 2049–2062, Aug. 2018.
- [45] X. Min, G. Zhai, K. Gu, Y. Liu, and X. Yang, "Blind image quality estimation via distortion aggravation," *IEEE Trans. Broadcast.*, vol. 64, no. 2, pp. 508–517, Jun. 2018.
- [46] X. Min, K. Ma, K. Gu, G. Zhai, Z. Wang, and W. Lin, "Unified blind quality assessment of compressed natural, graphic, and screen content images," *IEEE Trans. Image Process.*, vol. 26, no. 11, pp. 5462–5474, Nov. 2017.
- [47] International Telecommunication Union-Recommendations, Standard ITU-R BT.500-13, 2012, *Methodology for the Subjective Assessment of the Quality of Television Pictures*, Geneva, Switzerland.
- [48] D. J. Sheskin, *Handbook of Parametric and Nonparametric Statistical Procedures*, 4th ed. London, U.K.: Chapman & Hall, 2007.



Xianming Liu (M'12) received the B.S., M.S., and Ph.D. degrees in computer science from the Harbin Institute of Technology (HIT), Harbin, China, in 2006, 2008, and 2012, respectively. In 2011, he spent half a year at the Department of Electrical and Computer Engineering, McMaster University, Canada, as a Visiting Student, where he was a Post-Doctoral Fellow from 2012 to 2013. He was a Project Researcher at the National Institute of Informatics, Tokyo, Japan, from 2014 to 2017. He is currently a Professor with the School of Computer Science and Technology, HIT. He has published over 60 international conference and journal publications, including top IEEE journals, such as T-IP, T-CSVT, T-IFS, T-MM, T-GRS, and top conferences, such as CVPR, IJCAI, and DCC. He is a recipient of the IEEE ICME 2016 Best Student Paper Award.



Xiangyang Ji received the B.S. degree in materials science and the M.S. degree in computer science from the Harbin Institute of Technology, Harbin, China, in 1999 and 2001, respectively, and the Ph.D. degree in computer science from the Institute of Computing Technology, Chinese Academy of Sciences, Beijing, China. He joined Tsinghua University, Beijing, in 2008, where he is currently a Professor with the Department of Automation. His current research interests cover signal processing, image/video processing, and machine learning.



Gene Cheung (M'00–SM'07) received the B.S. degree in electrical engineering from Cornell University in 1995, and the M.S. and Ph.D. degrees in electrical engineering and computer science from the University of California, Berkeley, CA, USA, in 1998 and 2000, respectively.

He was a Senior Researcher at Hewlett-Packard Laboratories Japan, Ltd., Tokyo, Japan, from 2000 to 2009. He was an Associate Professor with the National Institute of Informatics, Tokyo, from 2009 to 2018. Since 2015, he has been an Adjunct Associate Professor at The Hong Kong University of Science & Technology. He is currently an Associate Professor with York University, Toronto, Canada.

His research interests include 3D imaging and graph signal processing. He has co-authored the Best Student Paper Award in the IEEE Workshop on Streaming and Media Communications 2011 (in conjunction with ICME 2011), the ICIP 2013, the ICIP 2017 and IVMSP 2016, Best Paper Runner-Up Award in the ICME 2012, and the IEEE Signal Processing Society Japan Best Paper Award 2016. He has served as an Associate Editor for numerous journals, including the IEEE TRANSACTIONS ON MULTIMEDIA (2007–2011), the IEEE TRANSACTIONS ON CIRCUITS AND SYSTEMS FOR VIDEO TECHNOLOGY (2016–2017), and the IEEE TRANSACTIONS ON IMAGE PROCESSING (2015–present). He served as a member of the Multimedia Signal Processing Technical Committee in the IEEE Signal Processing Society (2012–2014), and a member of the Image, Video, and Multidimensional Signal Processing Technical Committee [(2015–2017), (2018–2020)].



Debin Zhao received the B.S., M.S., and Ph.D. degrees in computer science from the Harbin Institute of Technology, China, in 1985, 1988, and 1998, respectively. He is currently a Professor with the Department of Computer Science, Harbin Institute of Technology. He has published over 200 technical articles in refereed journals and conference proceedings in the areas of image and video coding, video processing, video streaming and transmission, and pattern recognition.



Wen Gao (M'92–SM'05–F'09) received the Ph.D. degree in electronics engineering from the University of Tokyo, Japan, in 1991. He was a Professor with the Harbin Institute of Technology from 1991 to 1995, and a Professor at the Institute of Computing Technology, Chinese Academy of Sciences, from 1996 to 2006. He is currently a Professor in computer science at Peking University. He has published extensively, including five books and over 600 technical articles in refereed journals and conference proceedings in the areas of image processing, video coding and communication, computer vision, multimedia retrieval, multimodal interface, and bioinformatics.

Dr. Gao is a member of the Chinese Academy of Engineering, and a fellow of the ACM. He chaired a number of prestigious international conferences on multimedia and video signal processing, such as the IEEE ICME 2007, the ACM Multimedia 2009, the IEEE ISCAS 2013, and also served on the advisory and technical committees of numerous professional organizations. He served or serves on the editorial board for several journals, such as the IEEE TRANSACTIONS ON CIRCUITS AND SYSTEMS FOR VIDEO TECHNOLOGY, the IEEE TRANSACTIONS ON MULTIMEDIA, the IEEE TRANSACTIONS ON AUTONOMOUS MENTAL DEVELOPMENT, the EURASIP Journal of Image Communications, and the Journal of Visual Communication and Image Representation.